Influence of Lignin On Plastic Flow Deformation of Wood

Masako Seki (m-seki@aist.go.jp)
National Institute of Advanced Industrial Science and Technology Chubu Center Multi-Materials Research Institute: Sangyo Gijutsu Sogo Kenkyujo Chubu Center Multi-Material Kenkyu Bumon
https://orcid.org/0000-0001-5699-9376

Mitsuru Abe
National Institute of Advanced Science and Technology

Tsunehisa Miki
National Institute of Advanced Industrial Science and Technology

Masakazu Nishida
National Institute of Advanced Industrial Science and Technology

Research Article

Keywords: Wood, Plastic deformation, Deformability, Delignification, NMR

Posted Date: September 21st, 2021

DOI: https://doi.org/10.21203/rs.3.rs-893506/v1

Abstract

In this study, we clarified the influence of lignin in wood on its plastic flow deformation due to shear sliding of wood cells. Wood samples were subjected to delignification, where the lignin structure gradually changed, and characterized for their chemical and physicochemical properties, and deformability by free compression testing. The delignified wood deformed by efficient stretching and maintained its cell structures at a lower pressure compared to the untreated wood. The deformability was evaluated from two viewpoints: the initial resistance to plastic flow and final stretchability. The deformability of the delignified and untreated wood increased with increasing compressive temperature, even though the changes in molecular motility associated with the glass transition of lignin contributed minimally to the improvement in deformability. In the early stages of delignification, the molecular mass of lignin in the compound middle lamella decreased, which reduced the initial resistance to plastic flow. However, during the early stages of delignification, the stretchability of delignified wood was scarcely affected by changes in lignin. As the amount of lignin was further reduced and delignification proceeded in the vicinity of the polysaccharides, the stretchability significantly improved. The correlation between chemical and physicochemical properties and plastic flow deformability presented in this paper will be helpful for low-energy and highly productive forming of solid-state wood.

Introduction

The deformation processing of wood can effectively promote its use in various applications, such as furniture, building, construction, automotive, and other daily necessities. Some conventional methods of wood deformation include compression and bending processing using cell-wall deformations (Sandberg et al. 2012). These methods produce simple two-dimensional products while retaining the cell arrangement and structure of the wood. On the other hand, reducing the element size of wood can efficaciously enable the formation of more complex products. Wood-plastic composites (WPCs), which are a mixture of wood powder and plastic, are widely used as building materials (Spear et al. 2015). However, WPCs require an input of energy to miniaturize the wood, which results in the destruction of the original cell structure, such that the products do not retain the wood texture. Furthermore, in conventional processing, the element size of wood and the complexity of the product shape have a contradictory relationship. To date, the formation of a complex shape from solid-state wood has seen little success.

Recently, a new technique, wood flow forming (WFF), has been developed, which can form complex shapes with solid-state wood because it takes advantage of plastic flow deformation (Abe et al. 2020; Abe et al. 2021; Miki et al. 2014-1; Miki et al 2014-2; Miki et al. 2017; Seki et al. 2016; Yamashita et al. 2009). The wood is compressed in a heated mold, which enables it to plastically flow owing to the shear sliding between wood cells to produce a final shaped product (Miki et al. 2017). By applying the traditional plastic forming techniques used for metal and plastic materials, wood products can be efficiently produced in a short time. These techniques can maintain the original cell structure of wood, providing a unique cell-derived texture to the product (Miki et al. 2014-1). However, to improve the deformability of wood during the forming process and the durability of the products, it is necessary to

modify the wood by pretreatment before forming. The cell wall and compound middle lamella (CML) are modified by impregnating the wood with resin monomers (Miki et al. 2014-2; Seki et al. 2016) and/or chemical modification (Abe et al. 2020; Abe et al. 2021). WFF has great potential for various applications; however, it requires high temperatures (< 100°C) and pressures (< 50 MPa), making it energy-intensive and less productive. To solve these problems, this study focused on lignin, which acts as an adhesive and binds the polysaccharides (cellulose and hemicellulose) and cells together. In addition to the CML containing the highest amount of lignin, it is where plastic flow originates; therefore, lignin has a significant effect on plastic flow.

Delignification is a process that can remove lignin without breaking the cellular structure of the wood, and it has primarily been studied for pulping wood. However, in recent years, delignified wood (DW) (Kumar et al. 2021) has attracted attention as a functional material for use in transparent wood (Li et al. 2016; Li et al. 2017; Li et al. 2020), high-strength structural materials (Frey et al. 2019; Jakob et al. 2020; Song et al. 2018), high-performance thermal insulators (Li et al. 2018), and thermal energy storage materials (Montanari et al. 2019). Deformation processing that takes advantage of the flexibility of DW has also been developed (Khakalo et al. 2020; Frey et al. 2018; Frey et al. 2019). Frey et al. (2019) reported that a completely delignified veneer in a water-swollen state exhibited significant deformability in the fiber direction. However, the effect of delignification on the plastic flow deformation associated WFF has not been reported.

The thermal softening properties of water-swollen wood depend on the glass transition of lignin (Kojiro et al. 2008; Nakajima et al. 2009). When the molecular mass of lignin in wood decreases, its glass transition temperature also decreases, in turn significantly softening the wood (Nakajima et al. 2009). Therefore, it is expected that the changes in lignin due to delignification will promote the plastic flow deformation of wood and reduce the production energy required for WFF.

The objective of this study was to clarify the effect of lignin on the plastic flow deformation of wood. DW and untreated-wood (UW) samples with different molecular masses and amounts of lignin were prepared by subjecting them to delignification and varying the delignification time. Free compression testing was used to evaluate the deformability of the samples based on the initial resistance to plastic flow and final stretchability. The samples were characterized by attenuated total reflection infrared (ATR-IR) spectroscopy, nuclear magnetic resonance (NMR) spectroscopy, and dynamic viscoelastic measurements. The effects of the chemical structure and glass transition temperature of lignin on the plastic flow deformation of wood are also discussed.

Materials And Methods

Materials

Wood samples were successively cut in the longitudinal (L) direction from a block of sapwood of a Japanese cypress (*Chamaecyparis obtusa*) log collected from the Kiso region of Japan. The dimensions

of the samples used for the dynamic viscoelastic measurements were 1 mm (L) × 30 mm (radial (R) direction) × 3 mm (tangential (T) direction). The samples for the other measurements (ATR-IR, NMR, and free compression testing) were 5 mm (L) × 5 mm (R) × 5 mm (T). Prior to delignification, the wood samples were pre-treated with approximately 100°C distilled water for 4 h, followed by methanol for 6 h to remove the low-molecular-weight components. The pre-treated samples were then dried at 50°C for 18 h and 105°C for 2 h to a relatively constant mass (m_0). One side of the RT surface of some samples (5 mm × 5 mm × 5 mm) was microtome-finished prior to subsequent delignification.

Preparation of delignified wood samples

The pre-treated samples were delignified using 4 wt % sodium chlorite ($NaClO_2$) containing acetic acid solution (pH 3). The $NaClO_2$ solution was impregnated into the pre-treated samples under vacuum, and the impregnated samples were treated at 45°C for several reaction times (t_r) of 10, 30, 60, 180, or 360 min. Then, the DW samples were washed several times with distilled water and stored in water at 20–25°C Note that the DW sample with a t_r longer than 360 min was brittle and fragile; therefore, it was considered unsuitable for WFF and not evaluated in this study. In addition, the UW samples were impregnated with distilled water, instead of the $NaClO_2$ solution, at 20–25°C for 500 min or more (t_r: 0 min).

The area in the RT cross section of the water-swollen DW and UW samples (s_d and s_u, respectively) was measured, and the area increase rate (A_{RT}) of the water-swollen samples due to delignification was calculated using the following formula:

$$A_{RT} = (s_d - s_u) / s_u \times 100\ [\%]$$

Some of the water swollen samples were then dried at 35°C for 24 h, 50°C for 18 h, and 105°C for 3 h to a relatively constant mass (m_t). The mass loss (ML) due to delignification of the dried samples was calculated using the following formula:

$$ML = (m_o - m_t) / m_o \times 100\ [\%]$$

Attenuated total reflection infrared (ATR-IR) spectroscopy

The block-shaped sample (5 mm × 5 mm × 5 mm) in the dry state was cut in half in the L direction, and ATR-IR measurements were performed near the center of the cut surface (RT surface, that is, near the center of the wood sample). The ATR-IR spectra were measured on a Nicolet 6700 spectrometer (Thermo Scientific Inc., Waltham, MA, USA) at a 4 cm^{-1} resolution in the standard ATR mode; 32 scans were performed in the range of 4000–700 cm^{-1}.

Nuclear magnetic resonance (NMR) spectroscopy

Solid-state ^{13}C NMR spectra were measured on a Varian 400 NMR system spectrometer (Palo Alto, CA) with a Varian 4 mm double-resonance T3 solid probe. The dried samples were placed in a 4 mm ZrO_2

rotor spun at 15 kHz within a temperature range of 20–22°C. The ^{13}C cross-polarization and magic-angle spinning (CP-MAS) NMR spectra were collected with a 2.6 μs π/2 pulse at 100.56 MHz for the ^{13}C nuclei and a 40 ms acquisition period over a 30.7 kHz spectral width. Proton decoupling was performed with an 86 kHz ^{1}H decoupling radio frequency with a small phase incremental alteration (SPINAL) decoupling pulse sequence. The ^{1}H-^{13}C cross-polarization for the spectrum acquisition was conducted with a 5.0 s recycle delay in 1024 transients using a ramped-amplitude pulse sequence with a 2 ms contact time and a 2.6 μs π/2 pulse for the ^{1}H nuclei. The amplitude of the ^{1}H nuclei was linearly ramped down from 92.6% of its final value during the CP contact time. The ^{1}H spin-lattice relaxation time in the laboratory frame (T_1H) was indirectly measured by detecting the ^{13}C resonance enhanced by the cross-polarization in the ^{13}C CP-MAS sequence, and was applied after a π pulse to ^{1}H nuclei using the inversion recovery method. The T_1H analysis of the sample was carried out using the same solid-state probe used to obtain the ^{13}C CP-MAS NMR spectra of the sample at the same contact time and acquisition period.

Dynamic viscoelastic measurement

The temperature dependence of the loss tangent (tan δ) was measured by the tensile forced oscillation method using a thermomechanical analysis apparatus (TMA SS6100; Hitachi High-Tech Science Corp., Tokyo, Japan). The water-swollen sample (1 mm (L) × 30 mm (R) × 3 mm (T)) immersed in water was subjected to a temperature increase from 30°C to 100°C at a rate of 0.5°C/min. The frequencies for the measurement were 0.01 Hz; the span was 18 mm in the R direction; and the load amplitude was 70 ± 20 mN. Viscoelastic behavior is sensitive to the drying and heat history of the samples before the measurement (Kojiro et al. 2008). To unify the histories of the samples, they were heated to 100°C, naturally cooled down to approximately 20°C, and then subjected to measurements in the water-swollen state.

Free compression testing

A uniaxial compression test was carried out using a material testing machine (CATY TC-2kN-NS; Yonekura Mfg. Co. Ltd., Osaka, Japan) (Fig. 1). The testing machine equipped with a container enables horizontal compression tests of samples in a water-swollen state under confined heating conditions while recording load-stroke curves during hydrothermal compression. The compressive temperature (T_c) was controlled by heating the water with a cartridge heater immersed in a water pit.

The contained was sealed and heated until the temperature detected by the thermocouple stabilized to the target temperature (T_c). Then, the water-swollen sample was placed between the cylinders (diameter: 15 mm) under 2–3 N to ensure that the R was in the compression direction. The container was closed again to heat the sample to a constant temperature under saturated steam. Five minutes after achieving the temperature T_c, compression testing was conducted at a constant speed of 1 mm/min up to 3000 N of the maximum compression load or until the maximum stroke of 5 mm of the testing machine. The T_c was set to 40, 60, 80, and 100°C in consideration of the decrease in the glass transition temperature of

lignin due to delignification (Nakajima et al. 2009). Compression testing was conducted using three or more samples under the same conditions.

For one sample under each condition, the container was opened after compression testing, and the compressed sample was dried at room temperature to retain its shape while maintaining the stroke after testing, followed by further drying at 105°C for 1 h. Then, the mass (m_d) and thickness (r_c) in the compression direction were measured. The final compression ratio (C_d) was calculated as follows:

$$C_d = (r_b - r_c) / r_b \times 100\ [\%],$$

where r_b is the dimension in the R direction of the water-swollen sample before the compression testing. The appearance of the compressed sample from the LT planes was observed using an optical microscope (VHX-970F; Keyence Corp., Osaka, Japan). The area of the LT planes before and after compression testing was calculated by binarizing the captured image, and the area magnification (AM_d) was calculated as follows:

$$AM_d = A_c / A_b \times 100\ [\%]$$

where A_b and A_c are the areas of the LT planes of the water-swollen sample before compression and the dried sample after compression, respectively.

Results And Discussion

Characterization of untreated and delignified samples

The mass loss (ML) and the area increase rate (A_{RT})

Figure 2 shows the variation in *ML* (left axis, closed circles) and A_{RT} (right axis, open circles) as functions of delignification time (t_r). *ML* linearly increased with increasing delignification time, i.e., the lignin content of the wood sample decreased with delignification. Based on the original lignin content of cypress of 33 % (Pettersen 1984), approximately 40 % of the lignin was removed after 360 min of t_r. The A_{RT} also increased with increasing delignification time. The increase in the dimensions of the water-swollen sample was caused by the swelling of the cell wall and CML. The total volume of the adsorbed water in the cell wall and CML exceeded the volume of lignin removed by delignification.

ATR-IR spectroscopy

Figure 3 shows the ATR-IR spectra of the UW and DW samples, which indicate that the chemical structure of the wood sample changes with delignification. The area of the peak at 1490–1530 cm^{-1}, which corresponds to the skeletal vibrations of the benzene ring in lignin, decreased with increasing delignification time. This indicates the reaction is initiated during the early stages of delignification, as the benzene rings of lignin begin to disappear. The absorbance peak at 1725–1750 cm^{-1}, which

corresponds to the C = O stretch of lignin and hemicellulose, initially increased (t_r = 10 min), then decreased in the later stages (t_r = 360 min). The initial increase in this peak can be attributed to the reaction between $NaClO_2$ and lignin, which indicates that the aromatic ring was cleaved (Li et al. 2017). On the other hand, the decrease in the later stage was due to the decrease in the amount of lignin. The initial structural changes of lignin due to delignification consisted of the elimination and cleavage of the benzene ring, followed by the elimination of the benzene ring.

Solid state NMR measurements

Figure 4 shows the ^{13}C cross-polarization (CP)MAS NMR spectra for each substituent in the UW and DW samples. Signals corresponding to biomass constituents in the wood were assigned based on our previous report (Nishida et al. 2014). The carbohydrates appeared as relatively large and sharp signals in the range of 60–110 ppm. However, most of the signals for cellulose and hemicellulose, except cellulose C4, overlapped with each other, and the crystalline and amorphous signals for cellulose C4 and C6 could be separately observed. The aromatic and olefinic groups in lignin appeared as broader signals in the range of 110–160 ppm, while the methoxy groups in lignin appeared as isolated signals at 56 ppm.

During the early stages of delignification (t_r = 10 min), the signal intensity of the OCH_3 (56 ppm) and aromatic (110–160 ppm) groups in lignin rapidly decreased was observed. Meanwhile, the intensity of the C = O signal at a lower magnetic field (172 ppm) increased for 30 min, then gradually decreased as delignification progressed. The trends of the signal intensities for the aromatic and C = O groups in the ^{13}C CP-MAS NMR spectra were similar to those in the ATR-IR spectra. Therefore, in the first step of delignification, oxidation of the benzene ring of the guaiacyl unit on the surface of the lignin unit afforded two carboxyl groups at C3 and C4 positions (Hamzeh et al. 2008). Next, the cleavage of C–C and C–O bonds that provide bridging with other aromatic ring units at the inner site of the lignin resulted in higher ML of the delignified wood, because the oxidized portion was removed (Tarvo et al. 2010 and Qu el al. 2020). However, the signal pattern of the carbohydrates in the ^{13}C CP-MAS NMR spectra barely changed as a result of delignification, indicating that the chemical structures of cellulose and hemicellulose remained unchanged as delignification progressed.

Figure 5 shows the ^{1}H spin-lattice relaxation times in the laboratory frame (T_1H) of the dry samples. A minimal change was observed in the T_1H values at 65 and 75 ppm for t_r = 60 min, but tended to increase after 60 min. For wood in the dry state, the spin-lattice relaxation for each wood constituent occurs via lignin, which has the shortest T_1H value among the biomass constituents (Nishida et al. 2017). The increase in T_1H of the DW samples at t_r > 60 min was caused by the loss of lignin units with the short T_1H values. In the early stages (t_r < 60 min), delignification occurred at the distal part of the polysaccharide chain (for example, CML), with minimal effect on the polysaccharides. With increasing t_r (> 60 min), the reaction progressed toward the polysaccharide chain, resulting in an increase in the T_1H value because of the reduced interactions between the polysaccharides and lignin.

Dynamic viscoelastic measurement

Figure 6 shows the temperature dependence of tan δ for the water-swollen samples. The tan δ peak is attributable to the glass transition of lignin, and the peak temperature (Tg) in Fig. 6 corresponds to the glass transition temperature of lignin in the wood samples (Kojiro et al. 2008; Nakajima et al. 2009). As delignification progressed, the Tg gradually decreased and the shape of the peak broadened. These trends correspond well with those by Nakajima et al. (2009); they measured tan δ of Japanese cypress delignified by $NaClO_2$ and reported that the shift of Tg and the broadening of the tan δ peak were due to the decrease in the molecular mass and amount of lignin, respectively. The results in Fig. 6 demonstrate that the molecular mass and amount of lignin begin to decrease in the early stages of delignification (t_r: 10 min).

Deformability of untreated and delignified samples

Figure 7 shows the relationship between the nominal compressive stress (σ) and the compression ratio (C) during compression testing at each T_c. The σ slightly increased to a C of approximately 60% in all samples, during which the cell lumens in the wood samples gradually closed because of the buckling of the cell wall. As C increases, σ significantly increases at a constant rate, followed by an inflection point at which the rate of increase in σ decreases (indicated by the arrow in Fig. 7). These compressive behaviors were similar to those observed in our previous report (Miki et al. 2017). Before the inflection point, the cell lumens were completely closed and the sample was consolidated, resulting in a rapid increase in σ. After the inflection point, the rate of increase in σ decreased because the wood sample plastically deformed in the unconstrained direction (L or R). The inflection point was also detected in the flat region for t_r = 360 min at 100°C (shown by (d) $\bigtriangledown$); under this condition, plastic deformation occurred before the cell lumens were completely closed. The inflection points were not detected at 40°C, 60°C, and 80°C for t_r = 360 min and at 100°C for t_r = 180 min. This is because the inflection point due to the plastic deformation overlapped with the region denoting the rapid increase in σ.

The σ at the inflection point detected in Fig. 7 is the nominal compressive stress at the starting point of flow (σ_y), which indicates the initial resistance of the samples to plastic flow. Regardless of temperature, the longer the delignification time, the smaller the σ_y. Therefore, the delignification process reduced the initial resistance to plastic flow.

Figure 8 shows photographs of the samples that were dried after free compression testing to preserve their shape. After compression testing, all the samples were able to maintain their stretched state after drying by pressure; they only stretched in the T, and not in the L direction. Such anisotropy of plastic flow deformation is consistent with the phenomenon observed in our previous report (Miki et al. 2017). At high T_c, the sample that was delignification for a longer time exhibited the highest C_d of 91% (Fig. 8), indicating that a considerably thin product could be fabricated from solid-state wood.

Figure 9 shows an SEM image of the RT surface of the samples. None of the samples displayed cell wall destruction. Furthermore, evidence of mutual positional change between the cells was confirmed. The plastic flow deformation was mainly caused by the shear sliding phenomenon between the cells and at

the boundary of the CML, regardless of the difference in T_c and lignin state (such as quantity, quality, and molecular motility). The sample subjected to a longer delignification time (Fig. 7 (c, d)) displayed several slip surfaces, and plastic flow occurred in units with a smaller number of cells. The cells slightly protruding in the L direction were also observed, suggesting that delignification promoted slip deformation in the L direction.

Influence of lignin on plastic flow deformation of wood

Figure 10 shows the relationship between the *ML* by delignification of wood samples and σ_y, which indicates the initial resistance of wood samples to plastic flow. The higher the T_c, the lower the initial resistance to plastic flow. The initial resistance to plastic flow was logarithmically reduced to a *ML* of 4%, which indicates that the improvement in plastic deformability was significant in the early stages of delignification.

The final stretchability of the samples was evaluated using the AM_d. Figure 11(a) shows the relationship between *ML* and the AM_d of the wood samples. The AM_d increased with increasing T_c. The value of AM_d was almost unchanged during the early stages of delignification (*ML*: < 4%); however, as delignification progressed, AM_d remarkably increased and the sample was extensively stretched. The value of AM_d reached a maximum of 2.7 times for the longest t_r of 360 min at the highest T_c of 100°C. Furthermore, delignification caused a change in the density of the sample; therefore, the area per unit mass (A_d/m_d), which is an index of stretchability, was calculated based on the area of the LT surface (A_d) and the mass (m_d) of the dried compressed samples. The relationship between *ML* and A_d/m_d of the wood samples is shown in Fig. 11(b). The change in A_d/m_d depending on the T_c and the tendency toward *ML* were similar to those of AM_d (Fig. 11(a)). In contrast to the tendency of σ_y in Fig. 10, the stretchability did not increase during the early stages of delignification (*ML*: < 4%), but a significant increase was observed after a *ML* of 4% (t_r: > 60 min). Delignification with $NaClO_2$ initially proceeds from the lignin-rich CML during the early stages of the reaction and selectively softens the CML region. Then, the reaction and softening of the cell wall progresses during the later stages of the reaction (Xu et al. 2020). The results of T_1H in this study (Fig. 5) suggest that the lignin removal in the vicinity of the polysaccharide chains that make up the cell wall proceeds during the later stages of delignification (t_r > 60 min), which increases cell wall flexibility. Although the T_1H results of the dry state are represented, water was adsorbed between the constituents in the cell wall and CML during compression testing. Because the total volume of the adsorbed water on the cell wall increased as delignification progressed (Fig. 2), the adsorbed water acted as an intermolecular lubricant and contributed to the increase in stretchability. Therefore, the increase in stretchability that was observed during the later stages of delignification was likely due to the increased flexibility of the cell wall rather than the cleavage of the lignin network in the CML that occurred during the early stages of delignification. This flexibility of the cell wall generated many slip surfaces during plastic flow (Fig. 9 (c and d)).

A strong correlation is observed between the Tg (Fig. 6) and σ_y (Fig. 10), as shown in Fig. 12. This indicates that the reduction in the molecular mass of lignin significantly contributed toward the improved deformability observed during the initial resistance to plastic flow. Because the plastic flow of wood was shear failure originating from the CML (Fig. 9), structural defects in the CML generated during the early stages of delignification considerably affect the initiation of plastic flow.

In compression testing, at $T_c > T$g (filled circles) and $T_c < T$g (open circles), the molecular motility of lignin greatly differed because the lignin was in the glass and rubber states, respectively. Nevertheless, the different molecular motilities have minimal impact on the relationship between Tg and σ_y. Therefore, the influence of the molecular motility of lignin on the deformability was considered to be negligible.

Conclusion

We clarified the influence of lignin in wood on plastic flow deformation due to the shear sliding between wood cells. The ATR-IR and solid-state NMR spectroscopic analyses of delignification showed that the oxidative opening of guaiacyl ring on the surface of the lignin unit occurred in the early stages and the oxidized portion was released from the inner site of the lignin unit when delignification time was extended. Free compression testing was performed to evaluate the deformability (the initial resistance to plastic flow and final stretchability) of the samples. The decrease in the molecular mass of lignin in the CML that occurs in the early stages of delignification reduces the initial resistance to plastic flow deformation. However, the effect of changes in the chemical structure of lignin that occurred during the early stages of delignification on the final stretchability was relatively small. Furthermore, as the delignification progressed, the amount of lignin in wood decreased and the reaction reached the vicinity of the polysaccharide chains, resulting in a remarkable increase in stretchability. We also observed that an increase in T_c tends to improve the plastic deformability. However, the effect of the changes in molecular motility due to the glass transition of lignin on the deformability was very small. These results suggest that the molecular mass and amount of lignin in the CML and in the vicinity of the polysaccharide chains in the cell wall affect the plastic flow deformation of wood. Furthermore, the strategy of controlling the molecular mass and amount of lignin via delignification can yield more productive materials, as well as metal and plastic materials for achieving low-energy plastic flow deformation of wood. In this study, we examined delignified wood in the water-swollen state, but in the future, we plan to investigate the effect of other adsorbents, such as resin monomers, instead of water, on the plastic deformability of delignified wood.

Declarations

Funding (information that explains whether and by whom the research was supported)

This study was financially supported by Asahi Kasei Corporation.

Conflicts of interest/Competing interests (include appropriate disclosures)

The authors declare no conflict of interest.

Availability of data and material (data transparency)

The data that support the findings of this study are available from the corresponding author, Masako Seki, upon reasonable request.

Code availability (software application or custom code)

Not applicable

Additional declarations for articles in life science journals that report the results of studies involving humans and/or animals

Not applicable

Ethics approval (include appropriate approvals or waivers)

Not applicable

Consent to participate (include appropriate statements)

We agreed.

Consent for publication (include appropriate statements)

We agreed.

Acknowledgements

The authors like to thank the Asahi Kasei Corporation for financial support towards this study.

References

1. Abe M, Enomoto Y, Seki M, Miki T (2020) Esterification of solid wood for plastic forming. BioRes 15(3): 6282–6298. https://doi.org/ 10.15376/biores.15.3.6282-6298
2. Abe M, Seki M, Miki T, Nishida M (2021) Effect of the propionylation method on the deformability under thermal pressure of block-shaped wood. Molecules 26(12):3539. https://doi.org/10.3390/molecules26123539
3. Frey M, Biffi G, Adobes-Vidal M, Zirkelbach M, Wang Y, Tu K, Hirt AM, Masania K, Burgert I, Keplinger T (2019) Tunable wood by reversible Interlocking and bioinspired mechanical gradients: Moisture triggered reversible interlocking between neighboring cells. Adv Sci 6(10):1802190. https://doi.org/10.1002/advs.201802190

4. Frey M, Schneider L, Masania K, Keplinger T, Burgert I (2019) Delignified wood–polymer interpenetrating composites exceeding the rule of mixtures. Appl Mater Interfaces 11(38):35305–35311. https://doi.org/10.1021/acsami.9b11105
5. Frey M, Widner D, Segmehl JS, Casdorff K, Keplinger T, Burgert I (2018) Delignified and densified cellulose bulk materials with excellent tensile properties for sustainable engineering. Appl Mater Interfaces 10(5):5030–5037. https://doi.org/10.1021/acsami.7b18646
6. Hamzeh Y, Mortha G, Lachenal D, Izadyar S (2008) Selective degradation of lignin polymer by chlorine dioxide during chemical pulp delignification in flow through reactor. Polymer Plast Tech Eng 47:931–935. https://doi.org/10.1080/03602550802274506.
7. Jakob M, Stemmer G, Czabany I, Müller U, Gindl-Altmutter W (2020) Preparation of high strength plywood from partially delignified densified wood. Polymers 12(8):1796. https://doi.org/10.3390/polym12081796
8. Khakalo A, Tanaka A, Korpela A, Orelma H (2020) Delignification and ionic liquid treatment of wood toward multifunctional high-performance structural materials. Appl Mater Interfaces 12(20): 23532–23542. https://doi.org/10.1021/acsami.0c02221
9. Kojiro K, Furuta Y, Ishimaru Y (2008) Influence of histories on dynamic viscoelastic properties and dimensions of water-swollen wood. J Wood Sci 54:95–99. https://doi.org/10.1007/s10086-007-0926-4
10. Kumar A, Jyske T, Petrič M (2021) Delignified wood from understanding the hierarchically aligned cellulosic structures to creating novel functional materials: A review. Adv Sustainable Syst 5(5):2000251. https://doi.org/10.1002/adsu.202000251
11. Li Y, Fu Q, Yu S, Yan M, Berglund L (2016) Optically transparent wood from a nanoporous cellulosic template: Combining functional and structural performance. Biomacromolecules 17(4):1358–1364 https://doi.org/10.1021/acs.biomac.6b00145
12. Li Y, Fu Q, Rojas R, Yan M, Lawoko M, Berglund L (2017) Lignin-retaining transparent wood. ChemSusChem 10(17):3445–3451. https://doi.org/10.1002/cssc.201701089
13. Li K, Wang S, Chen H, Yang X, Berglund L, Zhou Q (2020) Self-densification of highly mesoporous wood structure into a strong and transparent film. Adv Mater 32(42):2003653. https://doi.org/10.1002/adma.202003653
14. Li T, Song J, Zhao X, Yang Z, Pastel G, Xu S, Jia C, Dai J, Chen C, Gong A, Jiang F, Yao Y, Fan T, Yang B, Wågberg L, Yang R, Hu L (2018) Anisotropic, lightweight, strong, and super thermally insulating nanowood with naturally aligned nanocellulose. Sci Adv 4(3):3724. https://doi.org/10.1126/sciadv.aar3724
15. Miki T, Seki M, Tanaka S, Shigematsu I, Kanayama K (2014) Preparation of three dimensional products using flow deformability of wood treated by small molecular resins. Adv Mater Res 856:79–86. https://doi.org/10.4028/www.scientific.net/AMR.856.79
16. Miki T, Sugimoto H, Shigematsu I, Kanayama K (2014) Superplastic deformation of solid wood by slipping cells at submicrometer intercellular layers. Int J Nanotechnol 11(5/6/7/8):509–519.

https://doi.org/10.1504/IJNT.2014.060572

17. Miki T, Nakaya R, Seki M, Tanaka S, Sobue N, Shigematsu I, Kanayama K (2017) Large deformability derived from a cell–cell slip mechanism in intercellular regions of solid wood. Acta Mech 228(8):2751–2758. https://doi.org/10.1007/s00707-015-1523-z
18. Montanari C, Li Y, Chen H, Yan M, Berglund L (2019) Transparent wood for thermal energy storage and reversible optical transmittance. Appl Mater Interfaces 11(22):20465–20472. https://doi.org/10.1021/acsami.9b05525
19. Nakajima M, Furuta Y, Ishimaru Y, Ohkoshi M (2009) The effect of lignin on the bending properties and fixation by cooling of wood. J Wood Sci 55:258–263. https://doi.org/10.1007/s10086-009-1019-3
20. Nishida M, Tanaka T, Miki T, Shigematsu I, Kanayama K, Kanematsu W (2014) Study of nanoscale structural changes in isolated bamboo constituents using multiscale instrumental analyses. J Appl Polym Sci 131:40243. https://doi.org/10.1002/app.40243
21. Nishida M, Tanaka T, Miki T, Hayakawa Y, Kanayama K (2017) Instrumental analyses of nanostructures and interactions with water molecules of biomass constituents of Japanese cypress. Cellulose 24:5295–5312. https://doi.org/10.1007/s10570-017-1507-3
22. Pettersen RC (1984) The chemical composition of wood. In: Rowell RM (ed.) The Chemistry of Solid Wood, Advances in Chemistry Series 207, American Chemical Society: Washington, DC, pp. 57–126
23. Qu Y, Yin W, Zhang RY, Zhao S, Liu L, Yu J (2020) Isolation and characterization of cellulosic fibers from ramie using organosolv degumming process. Cellulose 27:1225–1237. https://doi.org/10.1007/s10570-019-02835-w
24. Sandberg D, Haller P, Navi P (2012) Thermo-hydro and thermo-hydro-mechanical wood processing: An opportunity for future environmentally friendly wood products. Wood Mater Sci & Eng 8:64–88. https://doi.org/10.1080/17480272.2012.751935
25. Seki M, Kiryu T, Miki T, Tanaka S, Shigematsu I, Kanayama K (2016). Extrusion of solid wood impregnated with phenol formaldehyde (PF) resin: Effect of resin content and moisture content on extrudability and mechanical properties of extrudate. BioRes 11(3):7697–7709. https://doi.org/10.15376/biores.11.3.7697-7709
26. Song J, Chen C, Zhu S, Zhu M, Dai J, Ray U, Li Y, Kuang Y, Li Y, Quispe N, Yao Y, Gong A, Leiste UH, Bruck HA, Zhu JY, Vellore A, Li H, Minus ML, Jia Z, Martini A, Li T, Hu L (2018) Processing bulk natural wood into a high-performance structural material. Nature 554, 224–228. https://doi.org/10.1038/nature25476
27. Spear MJ, Eder A, Carus M (2015) 10 - Wood polymer composites. In: Ansell MP (ed) Wood Composites, 1st edn. Woodhead Publishing Elsevier Ltd.: Cambridge, UK, pp 195–249. http://dx.doi.org/10.1016/B978-1-78242-454-3.00010-X
28. Tarvo V, Lehtimaa T, Kuitunen S, Alopaeus V, Vuorinen T, Aittamaa J (2010) A model for chlorine dioxide delignification of chemical pulp. J Wood Chem Tech 30:230–268. http://dx.doi.org/10.1080/02773810903461476

29. Xu E, Wang D, Lin L (2020) Chemical structure and mechanical properties of wood cell walls treated with acid and alkali solution. Forests 11(1): 87. https://doi.org/10.3390/f11010087
30. Yamashita O, Yokochi H, Miki T, Kanayama K (2009) The pliability of wood and its application to molding. J Mater Proc Tech 209(12–13):5239–5244. https://doi.org/10.1016/j.jmatprotec.2008.12.011

Figures

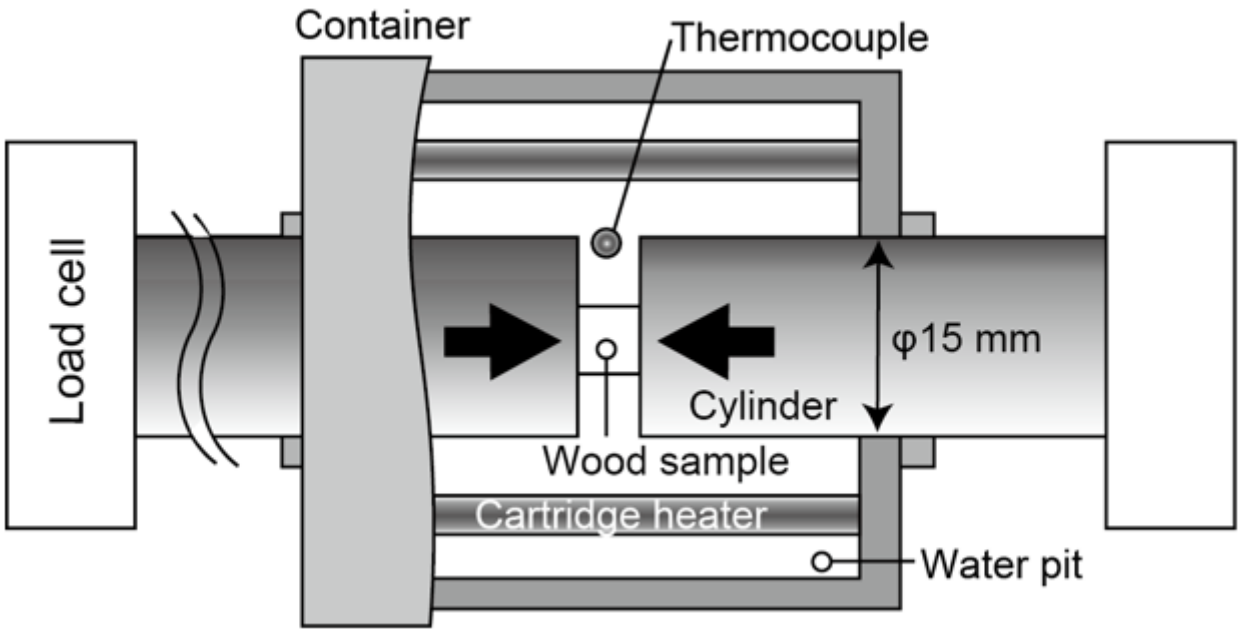

Figure 1

Schematic drawing of the experimental apparatus

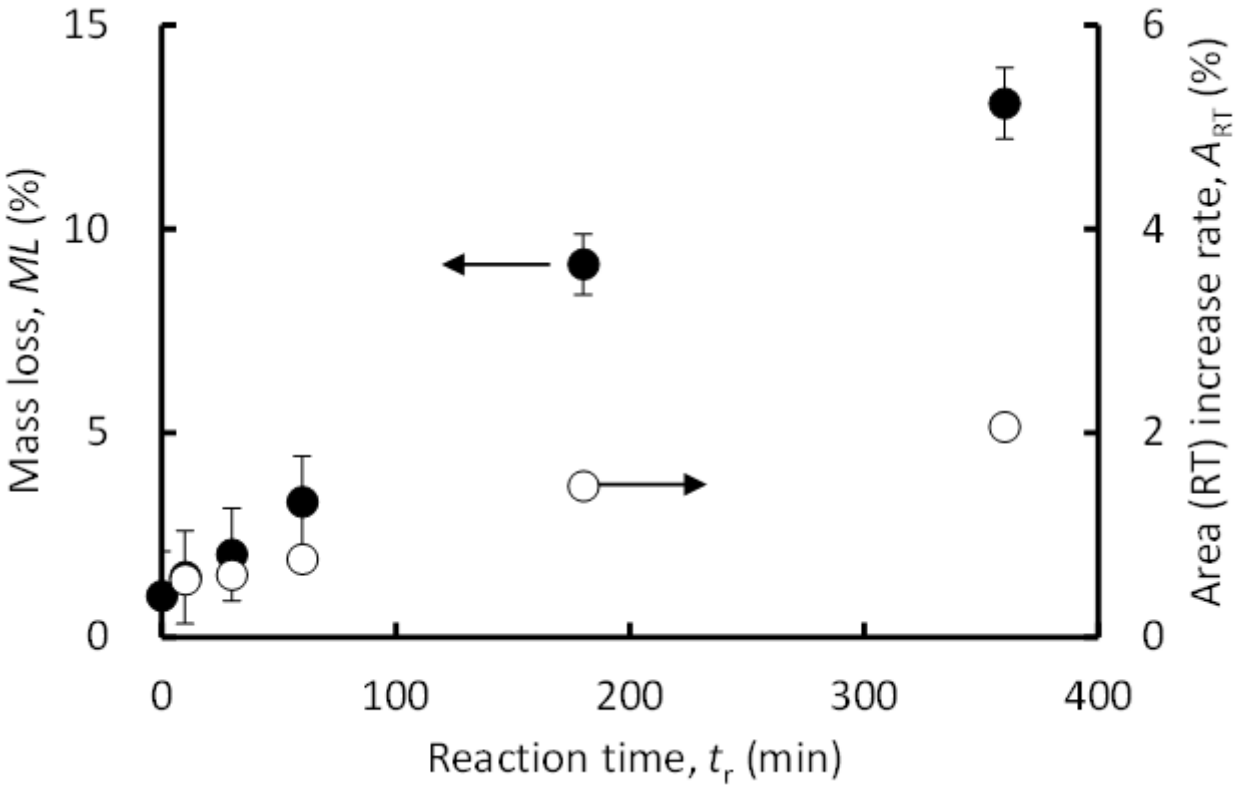

Figure 2

Variation of mass loss (ML) and area increase rate (ART) with delignification time (tr)

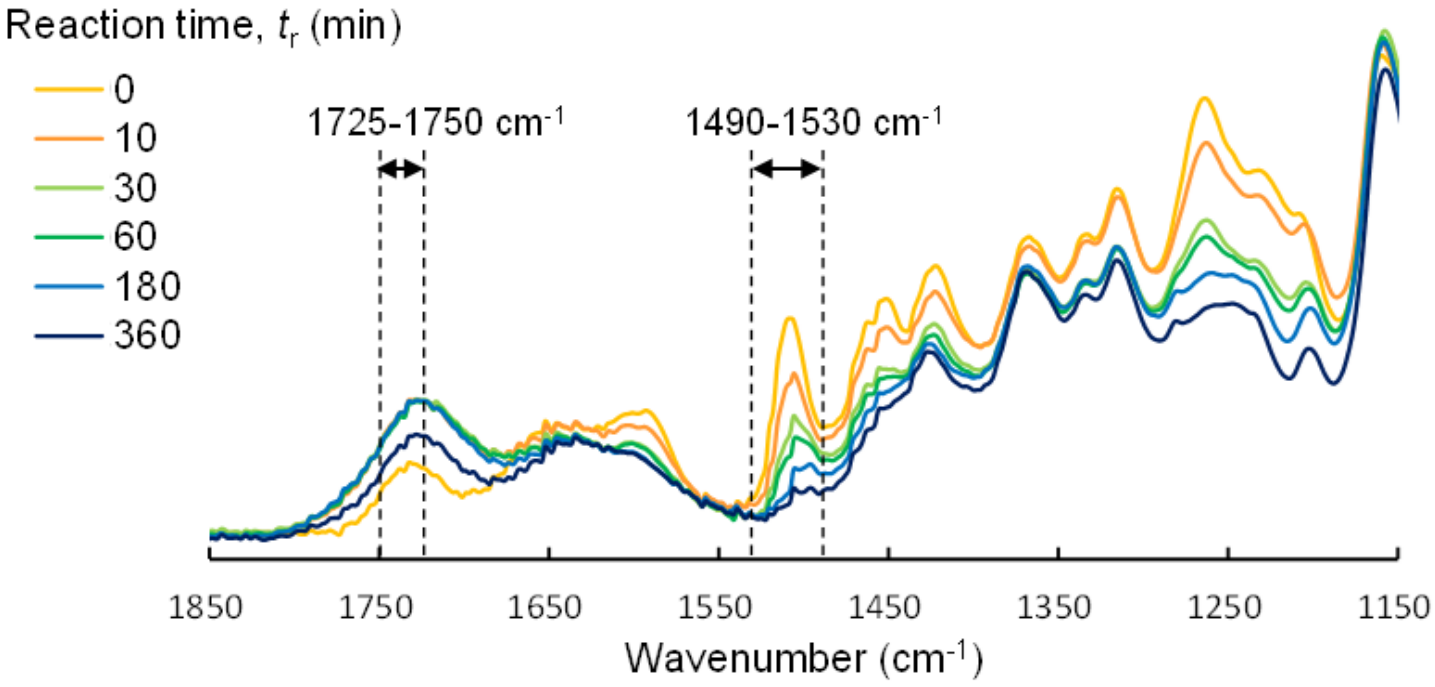

Figure 3

ATR-IR spectra of the untreated-wood (tr = 0 min) and delignified wood (tr = 10, 30, 60, 180 and 360 min) samples in the dry state

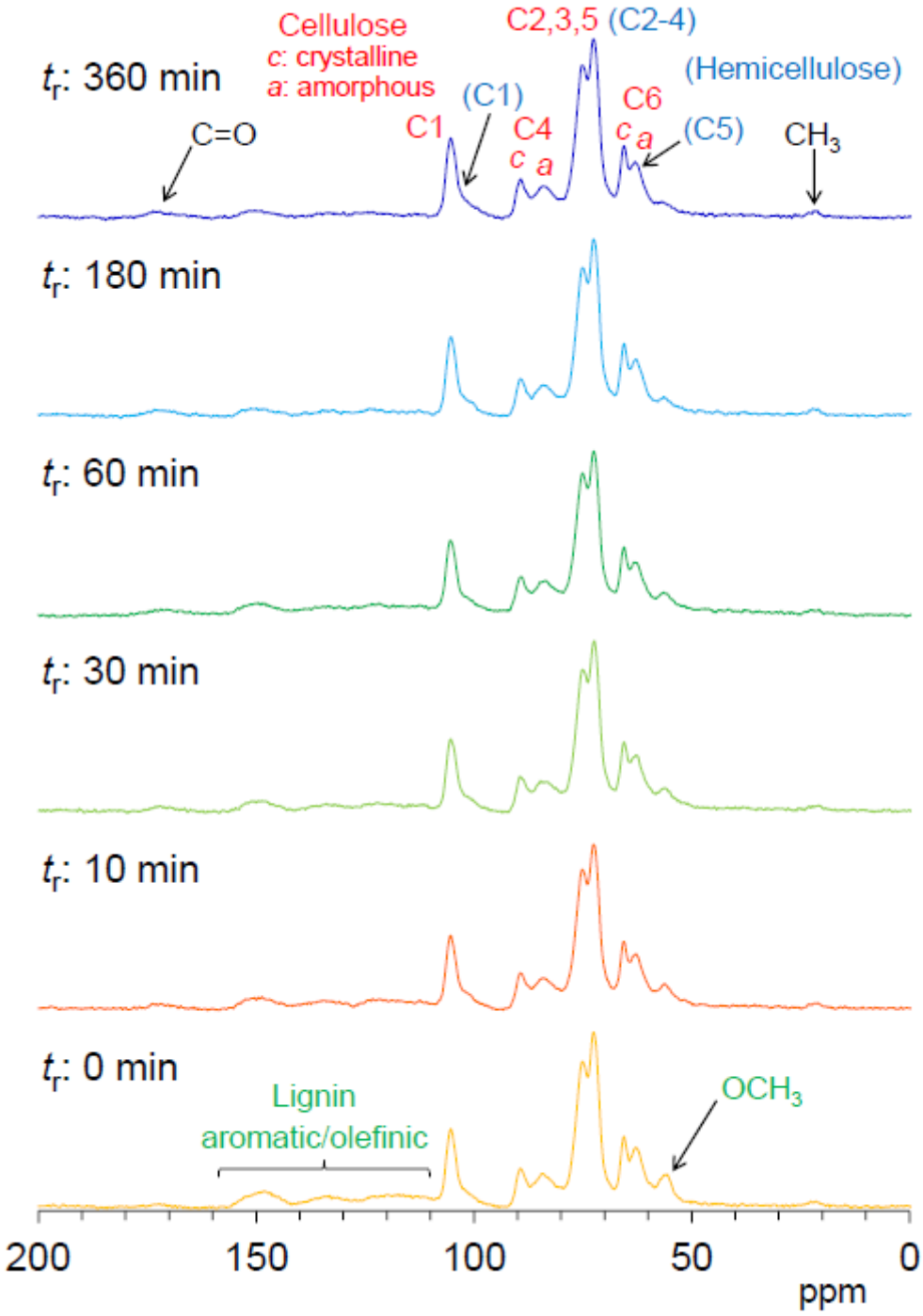

Figure 4

13C CP-MAS NMR spectra of untreated wood (tr = 0 min) and delignified wood (tr = 10, 30, 60, 180 and 360 min) samples in dry state

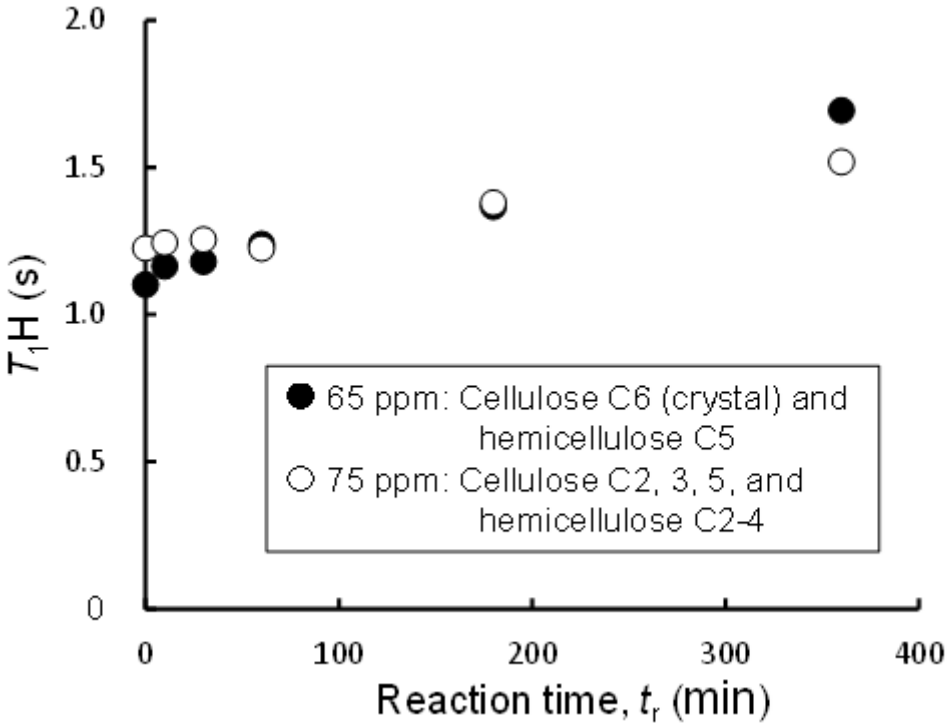

Figure 5

1H spin-lattice relaxation time in the laboratory frame (T1H) of the untreated wood (tr = 0 min) and delignified wood (tr = 10, 30, 60, 180 and 360 min) samples in the dry state at 65 and 75 ppm

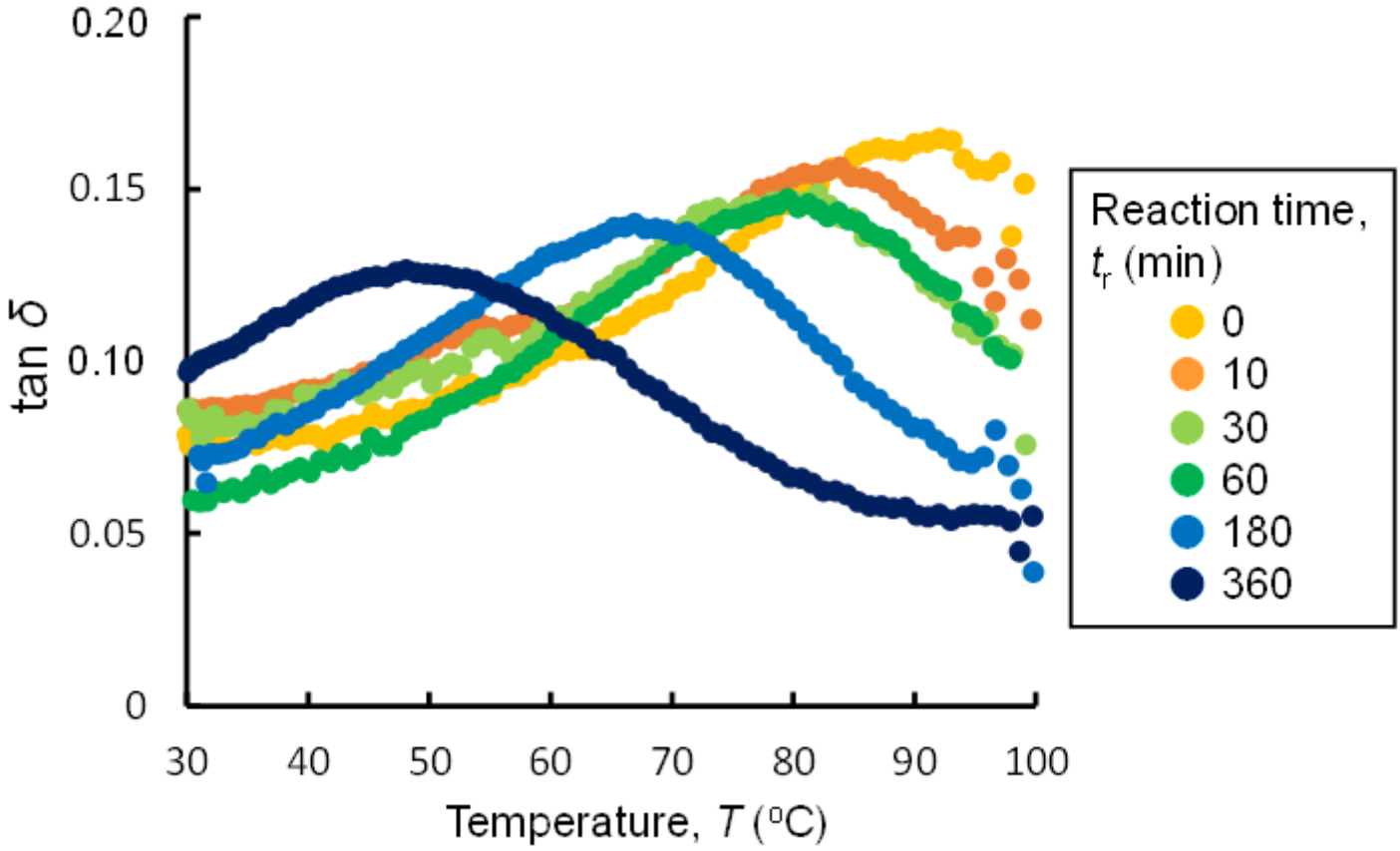

Figure 6

Temperature dependence of tan δ of untreated wood (tr = 0 min) and delignified wood(tr = 10, 30, 60, 180 and 360 min) samples in the water-swollen state

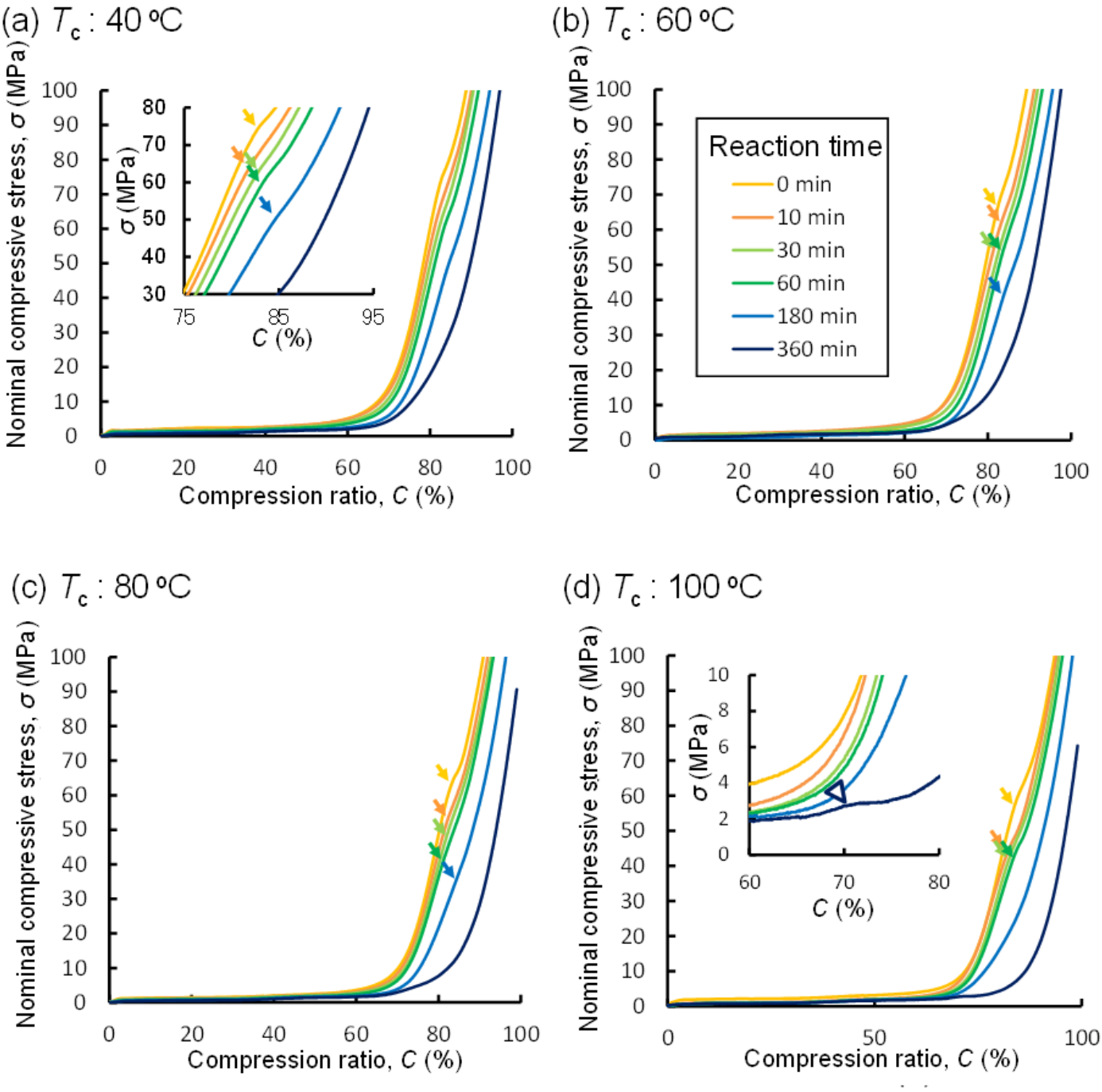

Figure 7

Relationship between the nominal compressive stress (σ) and compression ratio (C) during compression testing at each compressive temperature (Tc)

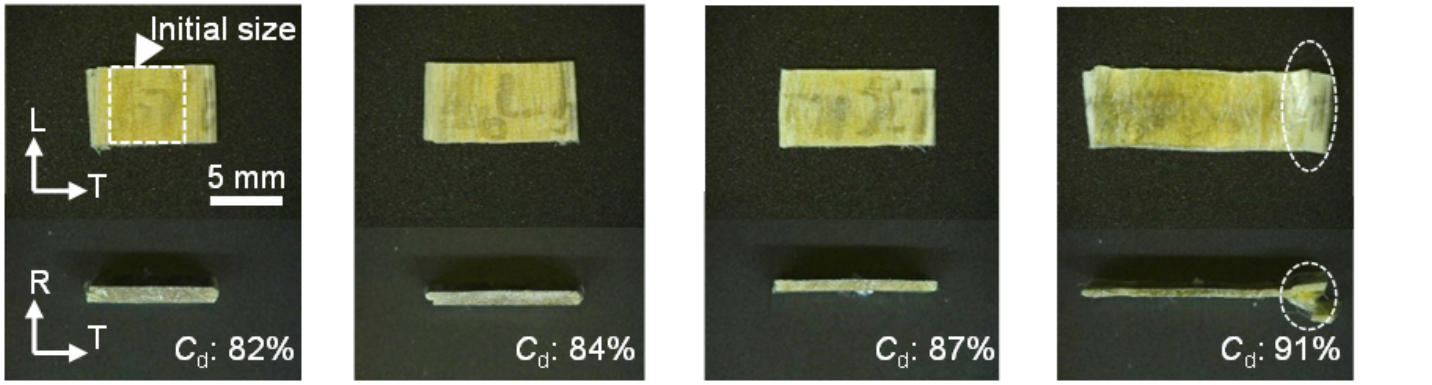

Figure 8

Photographs of the untreated wood (tr = 0 min) and delignified wood (tr = 360 min) samples whose shape was fixed by drying post-free compression testing. The final compression ratio (Cd) is shown in each photograph. The part surrounded by the dotted line of the circle shows the sample protruding from the cylinders of the testing machine

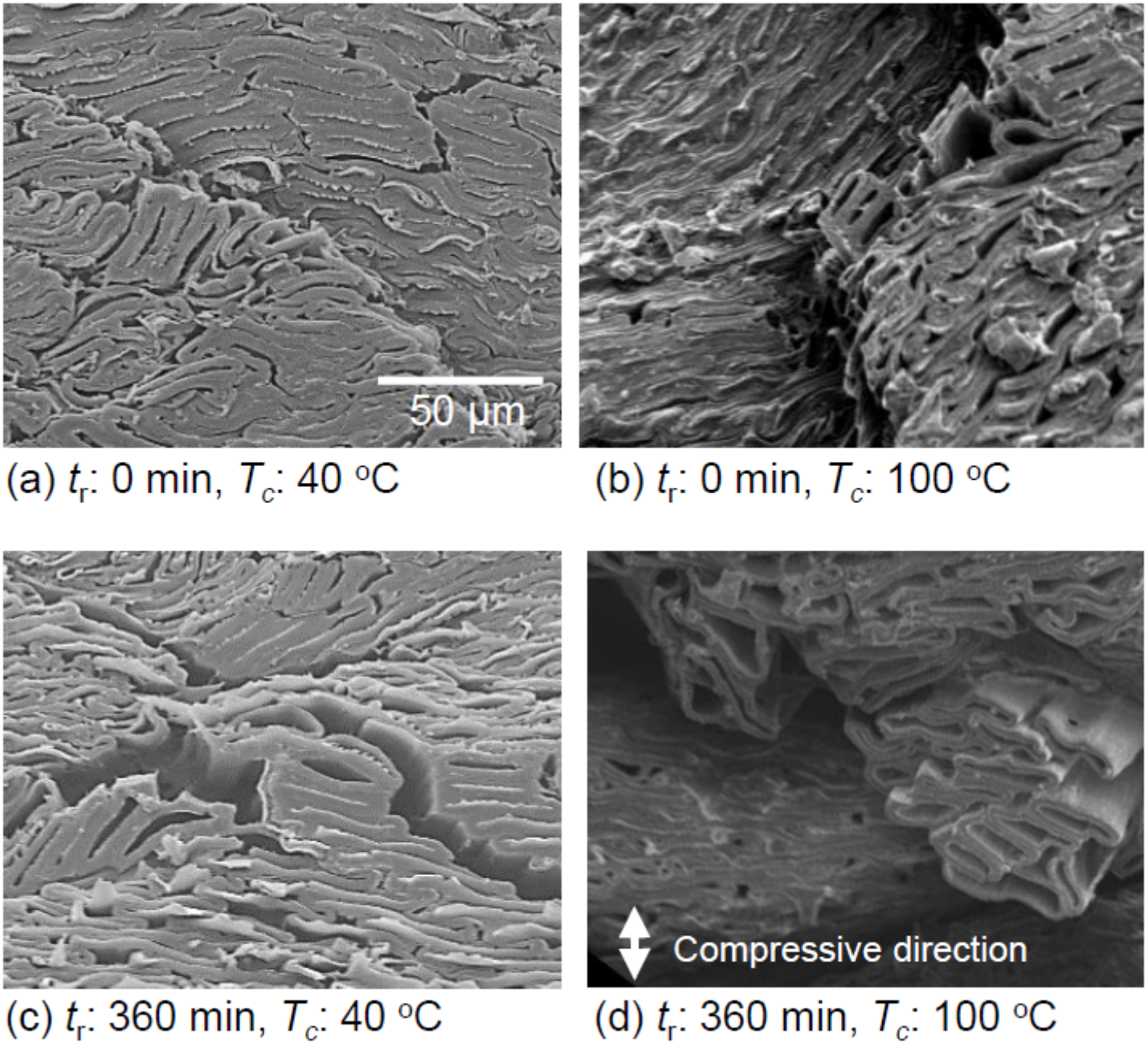

Figure 9

The SEM images of the radial-tangential surfaces of untreated wood (tr = 0 min) and delignified wood (tr = 360 min) samples after free compression testing

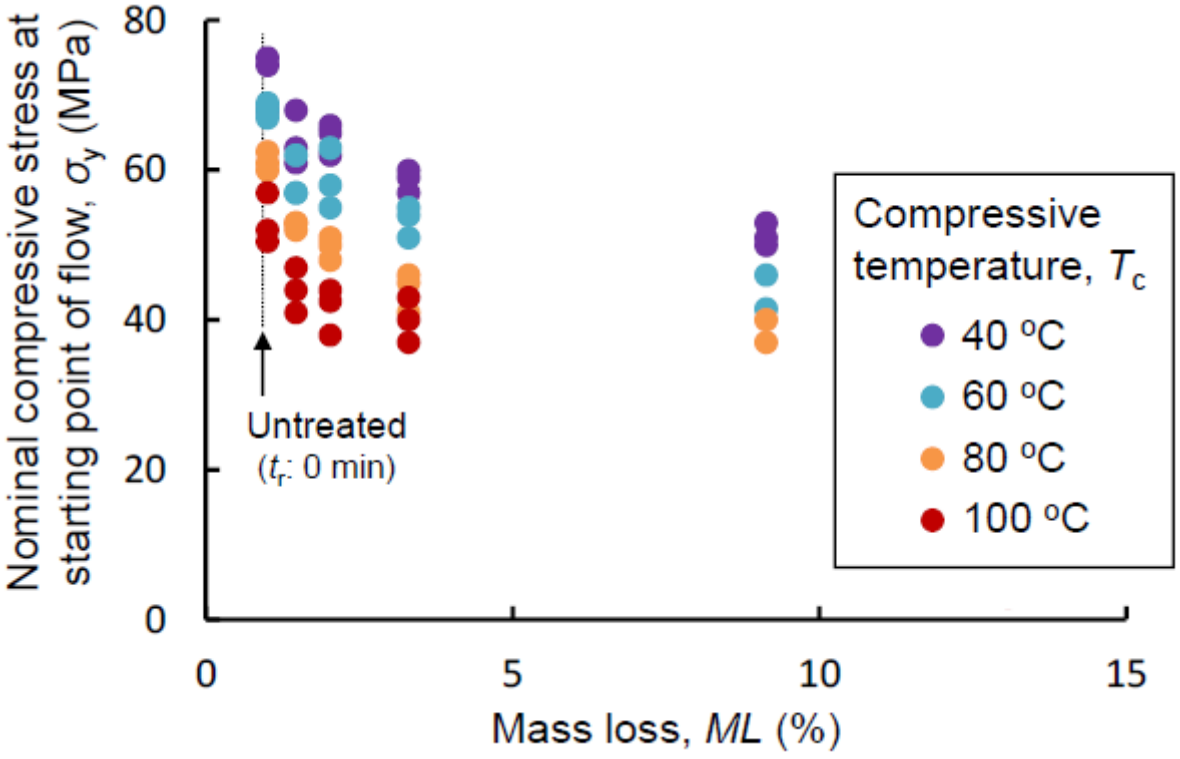

Figure 10

Relationship between the mass loss (ML) by delignification of wood samples and nominal compressive stress at starting point of flow (σy). The results of reaction time (tr) of 180 min at 100 °C and tr of 360 min were not described because the inflection point could not be detected after the consolidation of the sample in Fig. 7

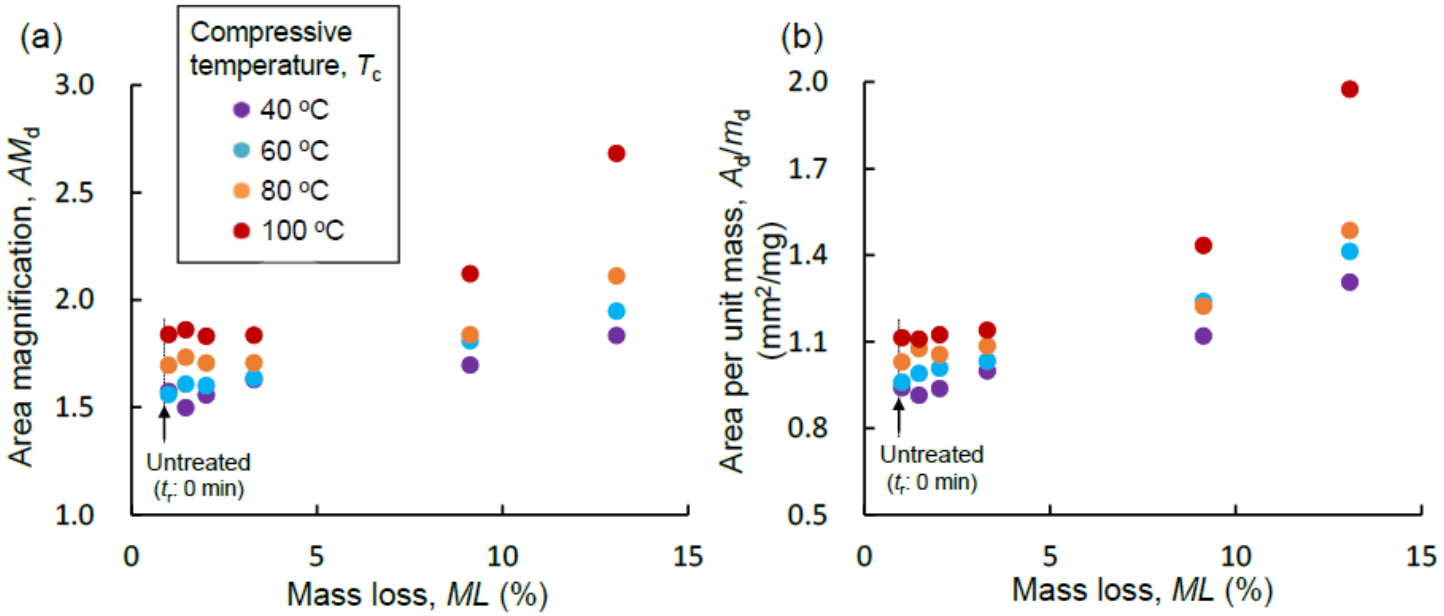

Figure 11

Relationship between mass loss (ML) by delignification and area magnification (AMd, a), and area per unit mass (Ad/md, b) of the wood samples

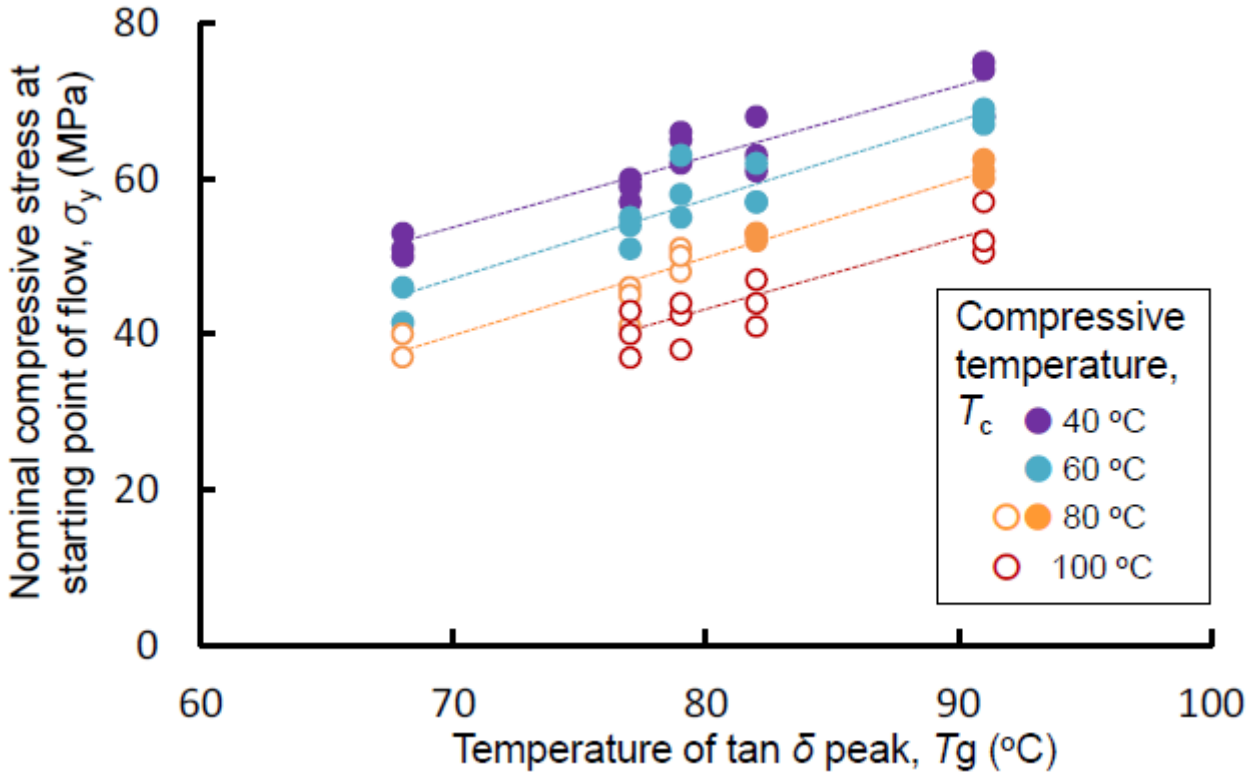

Figure 12

The relationship between the peak temperature of tan δ (Tg) from Figure 6 and the σy from Figure 10. Tg is the average of three measurements. Filled circles: Tc < Tg; open circles: Tc > Tg